JMEPEG (1999) 8:479-486

Pulsed Electrode Surfacing of Steel with TiC Coating: Microstructure and Wear Properties

A. Agarwal and N.B. Dahotre

(Submitted 30 October 1998; in revised form 22 January 1999)

In the present study, pulse electrode surfacing (PES) technique was employed to deposit ultrahard and wear-resistant titanium carbide (TiC) coating on AISI 1018 steel. Wear resistance of the coated surface increased significantly. An attempt was made to correlate the thermodynamic predictions and experimental observations. A composite coating that is adherent, crack free, and defect free in nature was obtained, with TiC being the most stable phase. Islands of TiC of various shapes and sizes are present in the Fe-rich matrix in the coating. Microhardness measurements suggest high hardness values in the coating region. Tribological properties such as wear resistance and coefficient of friction were also measured. The coefficient of friction data do not show significant fluctuations. Wear and friction phenomena in such a coating have been explained on the basis of a model based on composite/multiphase material.

Keywords 1020 steel, pulse electrode surfacing, surface engineering, TiC, wear resistance

1. Introduction

Surface engineering of the metallic substrates plays a vital role in enhancing their application in hostile environments. The monocarbides of group 4 such as TiC, ZrC, and HfC are ideal materials for increasing hardness, wear and erosion resistance, and corrosion and oxidation resistance of the metallic surfaces (Ref 1). Surface properties can be altered by depositing monocarbide ceramic coatings on the component without making changes in the bulk properties. Several techniques such as plasma spray, chemical vapor deposition (CVD), physical vapor deposition (PVD), detonation gun, laser-assisted processes, and electrolytic deposition are used to carry out these surface modifications (Ref 2-4). Pulse electrode surfacing (PES) is one of such surface modification techniques that utilizes high current electrical pulses of short duration to modify the metal surface (Ref 5-8). A unique combination of high-current and short-duration pulse by discharge capacitance-voltage circuit results in melting the ceramic electrode and depositing the material on the substrate. The primary requirement for the electrode material is that it should be electrically conductive and thus capable of melting in an electric arc.

The main advantage of this process is its ability to apply metallurgically bonded coatings with low heat input to the substrate at ambient temperature. This reduces the depth of the heat-affected zone (HAZ) and thermal distortion, hence minimizing the changes in the properties of the substrate material (Ref 6). The bulk substrate material remains near ambient temperature and acts as heat sink. Thus, there are no thermal stress effects or metallurgical changes in areas other than in the fusion zone. Since the bulk material acts as huge heat sink, heat is rapidly dissipated leading to rapid solidification of the molten pool. Such a high energy-density coating process results in a fine grained coating of high density, hardness, and strength. Since the coating is metallurgically bonded to the substrate, excellent adhesion properties of the PES coatings with high spalling resistance are achieved (Ref 9). Another advantage of the PES process includes the use of relatively inexpensive and portable equipment. PES coatings can be deposited in air at room temperature. This prevents the need for expensive environmental chambers required in several types of other coating processes. These ultrahard ceramic coatings are used for several applications such as nuclear, fossil, and geothermal energy environments, high temperature turbine coatings for aerospace applications, solid lubricants for high-vacuum industrial cutting tools, waste reclamation, water treatment plant, wear-resistant surfaces on large agricultural and textile equipment, high-temperature sensors, systems used in petrochemical and pharmaceutical industry, and modern sports equipment (Ref 2, 5-7, 9-11).

In the present study, TiC has been deposited on AISI 1018 steel using PES technique. Thermodynamic predictions were coupled with experimental analysis to characterize the TiC-Fe interface and coating morphology. Dry sliding wear tests were performed to evaluate the tribological properties of TiC coating deposited by PES technique.

2. Experimental Procedures

2.1 Materials

In the present study, TiC has been deposited on AISI 1018 steel using PES technique. TiC is a very hard refractory material finding increasing usage for wear-resistant applications such as bearings, nozzles, cutting tools, and jet engine blades. It has relatively low electrical resistivity and can be used as a conductor for electricity, especially at elevated temperatures. Thus, TiC is a suitable choice for deposit on a structural

A. Agarwal and **N.B. Dahotre,** Center for Laser Applications, Department of Materials Science and Engineering, University of Tennessee Space Institute, Tullahoma, TN 37388, USA.

material such as AISI 1018 steel using PES method. The salient properties of TiC and AISI 1018 steel are listed in Table 1 (Ref 1, 12).

2.2 Coating Process

TiC coatings were deposited on AISI 1018 steel coupon using PES method at Materials Modifications Inc. (MMI, Fairfax, VA). Coupons of AISI 1018 steel with dimensions of 25 by 25 mm were mechanically polished on emery paper of grit size 240 and then rinsed with acetone. A sintered electrode of TiC was used to deposit a coating on these steel coupons. The TiC electrode had 3 to 5 wt% Ni and 1 to 3 wt% Fe as binder. Deposition was carried out using a handheld gun in air at room temperature. Pulsed electrode deposition was carried out at a voltage of 50 V and spark time of 10 μs. The discharge capacitance used for the PES process was 450 μF with a current of 25 A.

2.3 Characterization

Coating morphology, interface, and surface topography were studied using a ISI Super III-A scanning electron microscope (SEM). Samples for metallography were prepared by polishing on a Buehler TEXMET 2000 cloth during initial stages of polishing. This reduced the damage to the dissimilar ceramic/metal interface during polishing. Nital (nitric acid + 10 vol% methanol) was used as the etchant for TiC-coated steel samples. Energy dispersive spectroscopy (EDS) analysis and x-ray elemental mapping were coupled with SEM to characterize the distribution of elements in a semiquantitative analysis.

Structural characterization was performed using a Philips Norelco x-ray diffractometer with Cu Kα radiation (1.54 Å), operating at 20 kV and 40 mA. Microhardness measurements were performed on a Buehler Micromet II microhardness tester using a Knoop indenter with normal load of 200 gm applied for 15 s. Tribological properties were measured using a block-on-disk tribometer. Coated coupons of dimension 25 by 25 mm were tested for dry sliding wear against a hardened steel ring rotating at a linear speed of 270 m/min. Weight loss measurements were made after successive 2 min. The dry sliding wear test was conducted for 10 min with an applied normal load of 2 kg. The coefficient of friction (μ) was also recorded simultaneously by an interfaced computer, which acquired data in the form of electrical output power of the motor. Even though data were recorded at a frequency of 1 Hz for a total test time of 10 min, an average of 10 successive points was taken for computing the coefficient of friction, μ.

Table 1 Salient physical properties of TiC and 1018 steel

Properties	TiC	Fe (1018 steel)
Crystal structure	*B*1 NaCl (cubic)	bcc
Melting point, °C	3065	1538
Density, g/cm^3	4.9	7.8
Lattice parameter, Å	4.33	2.89
Hardness, kg/mm^2	2800	250
Electrical resistivity, μΩ · cm	60	12
Thermal conductivity, W/m · K	27	55
Coefficient of thermal expansion, 10^{-6}/K	7.2	12.2

3. Results and Discussion

3.1 Thermodynamic Analysis and Predictions

The chemistry of the coating and interface is affected by the chemical reaction occurring within the deposited layer. These reaction products influence the mechanical and chemical properties of the coating. In the present study, therefore, attempts were made first to thermodynamically predict the possible reactions and secondly to verify the existence of these reaction products using analytical techniques such as energy dispersive x-ray spectrometry (EDS) and x-ray diffractometry.

For thermodynamic predictions, it is essential to consider all possible reactions for a ceramic-metal system. Thermodynamics of Fe-Ti-C system has been studied by several researchers (Ref 13-15). Even though to date, much work continues toward understanding Fe-Ti-C interaction, far from a thorough understanding has been achieved (Ref 15). It has been concluded that Fe-Ti-C is a very active and complex system due to several factors (Ref 13-15). This is mainly due to the presence of carbon, which easily migrates from TiC to Fe and vice versa depending upon reaction conditions such as temperature and activities of the elements (Ref 13-14, 16). This is further corroborated by the Ti-C phase diagram, which shows that TiC_x (x is ≤1) exists as a single homogeneous carbide phase for a wide range of stoichiometry (Ref 1). Hence, it provides a variable activity of carbon in the melt, which, in combination with temperature, influences the possible reactions in the melt zone. However, in an earlier similar study where TiB_2 was deposited on AISI 1018 steel using PES technique, it was found that unlike the Fe-Ti-C system, the Fe-Ti-B is not an active system (Ref 17). For the Fe-Ti-C system, possible reactions between Ti-C, Fe-Ti, and Fe-C are being considered. From the binary phase diagrams (Ref 18), the following reactions are possible. Thermodynamic data such as free energy of formation are extracted from various sources (Ref 19).

Ti-C system:

$$Ti + C = TiC_x$$

$$\Delta G = -182.9 + 0.01\,T \text{ kJ/mol} \quad (298\text{ K} < T < 1155\text{ K})$$

$$\Delta G = -186.4 + 0.013\,T \text{ kJ/mol} \quad (1155\text{ K} < T < 2000\text{ K})$$

The existence of Ti_2C and TiC_2 has not been confirmed (Ref 1).

Fe-C system:

$$3Fe + C = Fe_3C$$

$$\Delta G = 25.92 - 0.023\,T \text{ kJ/mol} \quad (298\text{ K} < T < 463\text{ K})$$

$$\Delta G = 26.67 - 0.025\,T \text{ kJ/mol} \quad (463\text{ K} < T < 1115\text{ K})$$

$$\Delta G = 10.34 - 0.01\,T \text{ kJ/mol} \quad (1155\text{ K} < T < 1808\text{ K})$$

$$2Fe + C = Fe_2C$$

$$\Delta G = 19.86 - 0.01\ T\ \text{kJ/mol}\ (298\ \text{K} < T < 1115\ \text{K})$$

$$\Delta G = 18.42 - 0.01\ T\ \text{kJ/mol}\ (1155\ \text{K} < T < 1808\ \text{K})$$

Fe-Ti system:

$$Fe + Ti = FeTi$$

$$2\ Fe + Ti = Fe_2Ti$$

Gibbs free energy data are not available for FeTi and Fe_2Ti. Lack of such data makes thermodynamic stability predictions difficult for many systems. Henceforth in this article, discussion is limited to TiC_x, Fe_2C, and Fe_3C. Figure 1 shows the free energy of formation of carbides as a function of temperature. It is evident from the graph that TiC is the most stable carbide, and free energy of formation does not change significantly with temperature. This implies that the entropy (obtained from the slope of the curve) of formation of carbides is almost negligible. Hence, it is reasonable to assume that free energy of carbides varies in a similar manner even at the temperature attained during arc formation in PES process. It is also evident from Fig. 1 that some possibility of formation of Fe_3C exists at temperatures higher than 1100 K. It is noteworthy that apart from temperature, activity of carbon also plays an important role in formation of various reaction products (Ref 13-16). In the earlier work it has been shown that at higher temperatures TiC dissociates into Ti and C increasing the activity of carbon in the melt (Ref 14-16). This results in some of the carbon diffusing into the Fe melt to form Fe_3C whereas the remaining carbon recombines with Ti to reprecipitate stoichiometric TiC.

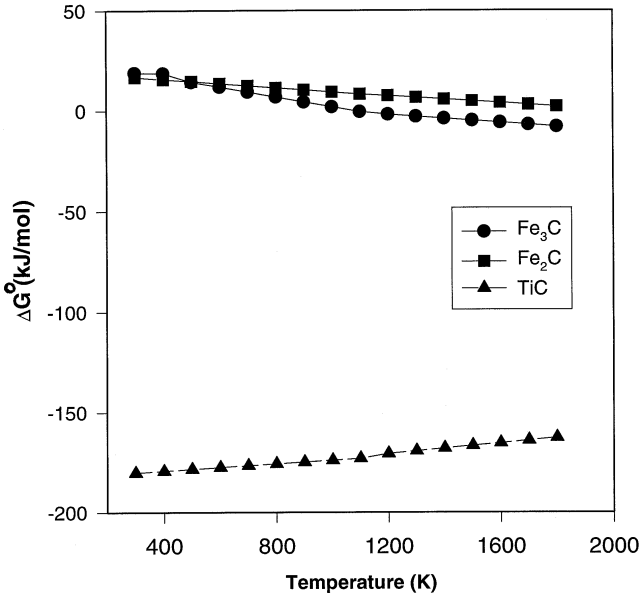

Fig. 1 Gibbs free energy of formation of carbides of Fe and Ti as a function of temperature

However, excess Ti remains in the Fe melt as Fe-Ti eutectic or solid solution (Ref 14-16).

3.2 Microstructural Characterization

The topographical features of the top surface of TiC deposited on AISI 1018 steel are shown in Fig. 2. The surface is irregular with a splash appearance. It is a characteristic feature of PES process. Electrical energy melts the TiC electrode and forms a molten globular droplet on the tip of the electrode. Molten droplet impinges on the steel substrate and produces a splash like appearance. Such process of mass transfer from electrode to substrate is supported by the fact that the PES process was carried out in air. Dissociable gases like air and nitrogen form a plasma of high thermal conductivity, which promotes globular mass transfer (Ref 5).

Figure 3 shows the SEM micrograph of the cross-section of TiC coated 1018 steel. Although coating thickness is not

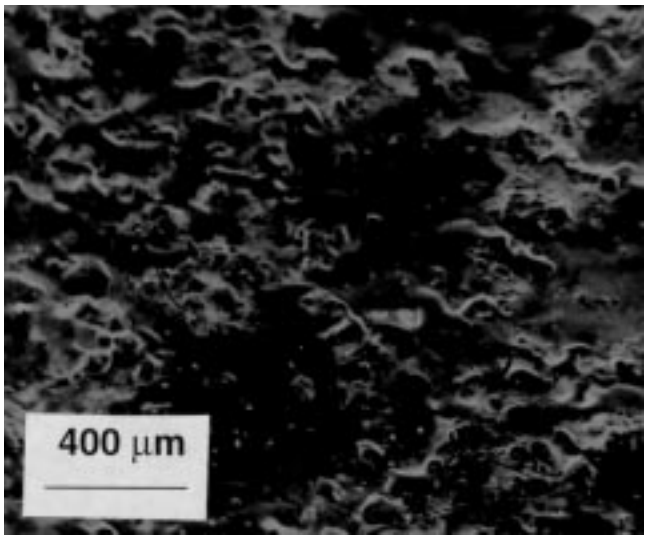

Fig. 2 SEM micrograph showing the topographical features of pulse electrode surfacing (PES) deposited TiC coating on steel

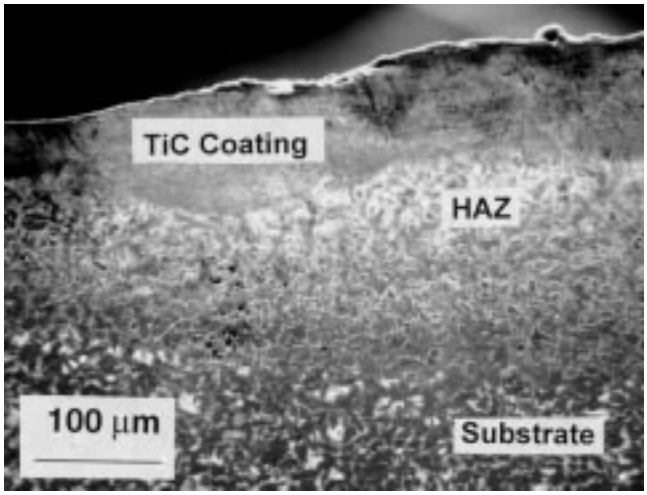

Fig. 3 SEM micrograph of the cross section of TiC deposited steel coupon

uniform, it is dense, adherent, and free from defects such as cracks and porosities. The irregular coating thickness is in accordance with the nature of the PES process as observed in the topographical features shown in Fig. 2. A strong, continuous, and adherent interface along with the HAZ is illustrated in Fig. 4(a). Lath-shape martensite is also formed in the HAZ. Islands (particles) of TiC of various size and shape within the coating are observed in Fig. 4(a) and 5. The coating is composite in nature with TiC islands acting as hard reinforcement in a matrix of Fe and Ti. Most of these TiC islands have irregular morphology. It has been postulated that some of TiC particles dissociate and reprecipitate from the melt, leading to in situ formation of islands of TiC of various shape and size (Ref 13-14, 16).

The presence of Ti and Fe in the coating is evident from elemental x-ray maps of the cross section corresponding to Ti and Fe distribution in Fig. 4(b, c), respectively. TiC islands (particles) are shown by a Ti-rich zone in the x-ray maps, whereas the matrix contains mostly Fe and a small amount of Ti. EDS quantitative analysis shows the presence of up to 5 to 25 wt% Ti in the matrix at various locations. Figure 6 is the EDS spectrum corresponding to matrix location within the composite coating region. The reason for high Fe content is due to the large difference between the melting points of TiC coating and the Fe substrate. The lower melting point constituent (i.e., Fe) forms a larger volume of molten material as compared to the TiC electrode. This results in high concentration of Fe in the deposited layer (Ref 17).

Fe has excellent wetting and binding properties for refractory ceramic like TiC and TiB_2 (Ref 20, 21). Based upon electronic configuration of *d* electron subshells in transition metals and their hard refractory alloys, an empirical rule has been suggested that allows selection of a suitable binder for given refractory material (Ref 20). This has been corroborated by several researchers for several material systems such as (Ti,Ta)C-Mo and TaC-Ni (Ref 22). Also, in an earlier study conducted by the present authors where TiB_2 was deposited on AISI 1018 steel using PES method, it was observed that Fe acts as an excellent binder for TiB_2 (Ref 17). This further validates the hypothesis of empirical rule suggested for the choice of binder for transition metal based refractory ceramic. Moreover, TiC particles wet Fe easily at high temperatures and wetting increases at high temperatures (Ref 14, 23). All these factors illustrate the role of Fe as an excellent binder for TiC.

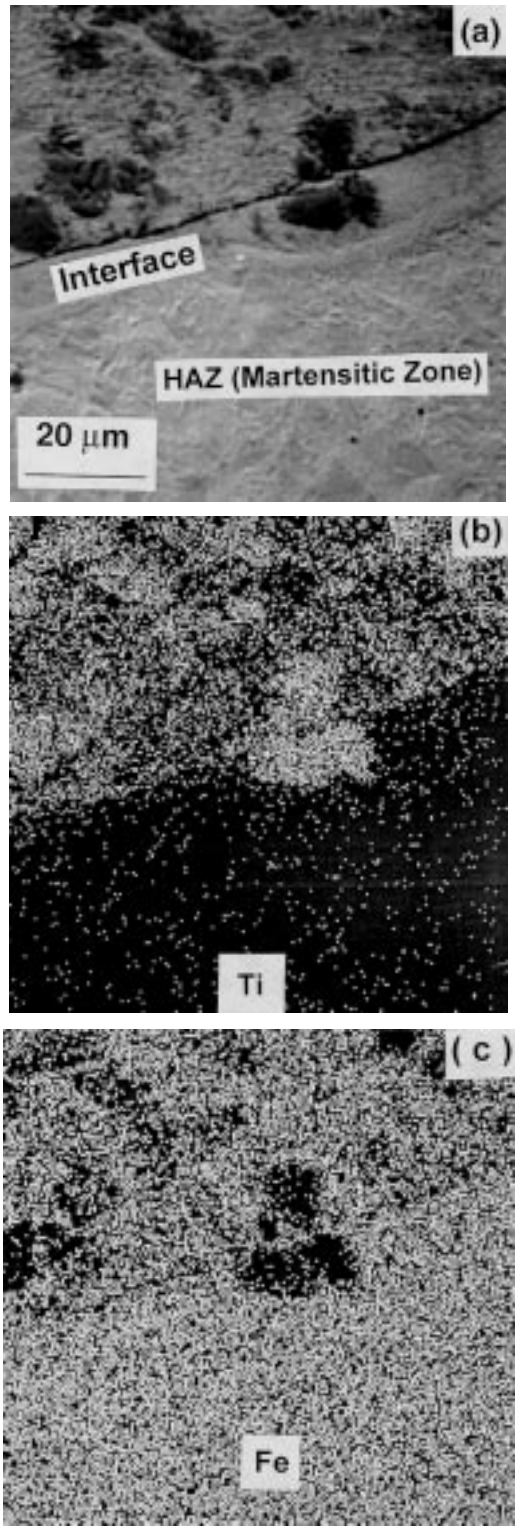

Fig. 4 (a) SEM micrograph of the interfacial region of TiC-deposited steel coupon and corresponding x-ray elemental map for (b) Ti and (c) Fe

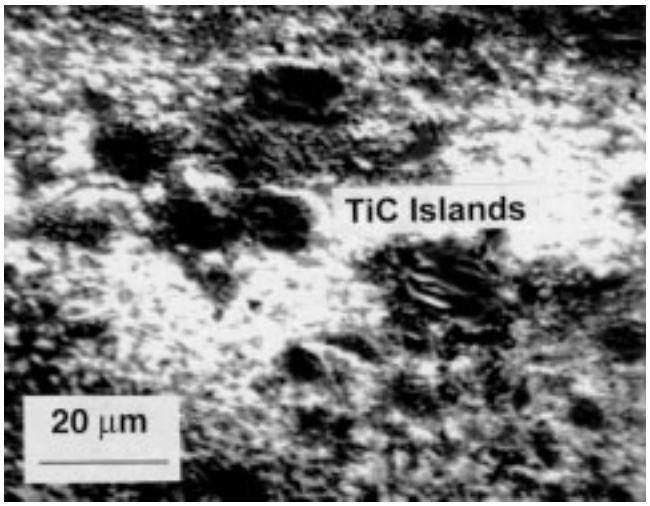

Fig. 5 High magnification SEM micrograph showing TiC islands of various shapes and sizes in the coating region

The presence of Ti in the matrix could possibly be due to the following reasons. Excess Ti from TiC_x gets dissolved in the Fe melt and remains as Fe-Ti solid solution or Fe-Ti-C eutectic (Ref 16). However, the presence of 5 to 25 wt% Ti in the melt exceeds the solid solubility limits, which could be attributed to the nonequilibrium processing experienced during PES processing. Such higher compositions under nonequilibrium processing have also been observed earlier (Ref 24). Figure 7 illustrates the x-ray diffraction spectrum of the coated surface. It shows all the peaks of TiC, Fe (ferrite), and Fe (austenite). There is also an indication of possible FeTi formation, as FeTi peak overlaps with Fe (austenite) peak. Formation of such phase also accounts for high weight percent of Ti present in the matrix. FeTi formation in Fe-Ti-C system has also been observed in earlier studies (Ref 24). Austenite peaks exist because Fe melt retains excess carbon due to rapid solidification. On the contrary, carbon contents might not be high enough to form Fe_3C. This is also corroborated by the absence of Fe_3C peaks in Fig. 7. Furthermore, it has been shown earlier in thermodynamic predictions of Fig. 1 that free energy of formation of Fe_3C does not support its formation. Thus, TiC is the major phase in the coating in addition to Fe.

3.3 Mechanical Characterization

Mechanical characterization of the coating and interface was performed using a microhardness tester. Figure 8 shows a SEM micrograph of the cross section of the coating and the HAZ with microhardness indentations. The relative difference in the size of microhardness indentations explains the variation in hardness. Microhardness values (Knoop) in the coating are high with an average value of 1235 ± 86, and they drop down to 352 ± 32 in the HAZ. Microhardness in unaffected base material is 172 ± 12. Such variation in hardness is attributed to the presence of TiC particles in the coating and martensite in the HAZ as observed in Fig. 8. There is no crack initiation or delamination at the site of indentation, which indicates the tough nature of the coating. It should also be observed that though TiC and Fe show considerable differences in their coefficients of thermal expansion, still there is no delamination at the TiC/Fe interface. Such toughness combined with high hardness is attributed to the composite nature of the coating. Thus, TiC particles embedded in an Fe-rich matrix produces an effect similar to that of the WC-Co system.

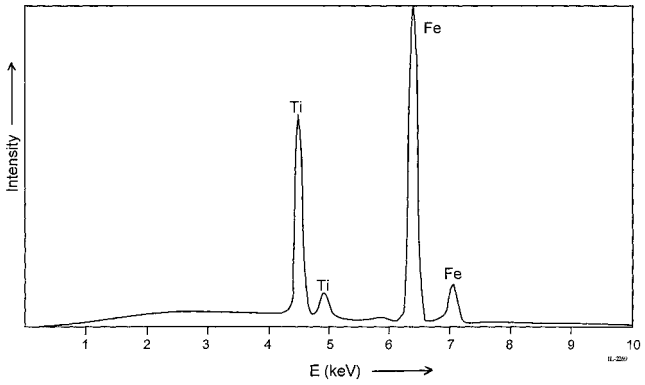

Fig. 6 EDS spectrum of the matrix region within the composite coating

3.4 Tribological Characterization

Wear Test (Weight Loss Analysis). Wear test results are presented in Fig. 9, which shows the weight loss over a 10 min period. It can be easily observed that the coated surface shows excellent wear resistance in comparison to uncoated AISI 1018 steel substrate. Wear rate (g/min) of the coated surface has reduced by almost a factor of 4, and it tends to stabilize after an initial period of 4 min. This suggests a formation of wear-resistant film over the entire substrate. The worn surface was subjected to topographic observations in SEM. Figure 10(a) shows a low magnification SEM micrograph of the worn surface of TiC coated AISI 1018 sample. Elemental x-ray maps corresponding to Ti and Fe distribution in Fig. 10(a) are presented in Fig. 10(b, c), respectively. These show Ti presence all over the surface along with Fe, which is in accordance with the composite

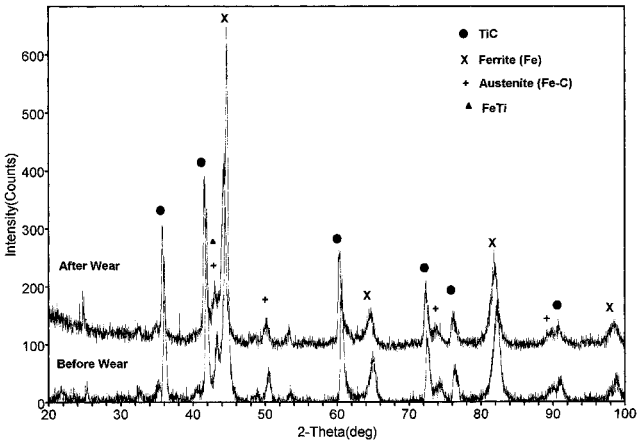

Fig. 7 X-ray diffraction spectra before and after wear of TiC deposited steel coupon

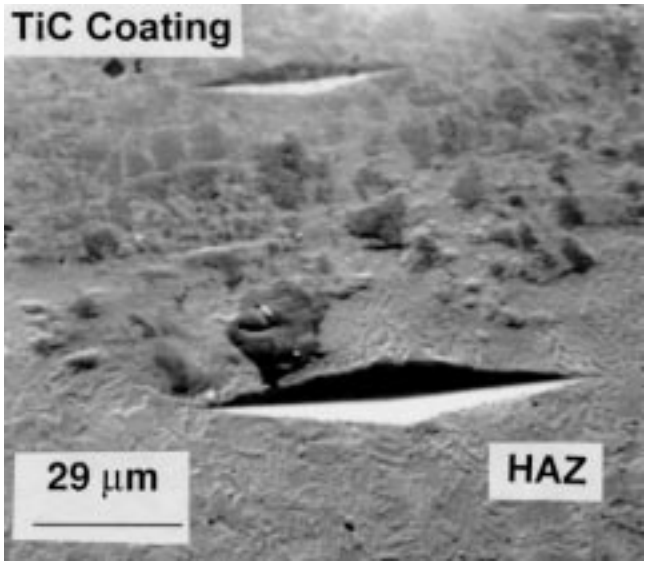

Fig. 8 SEM micrograph of the cross section showing microhardness indentations at different locations

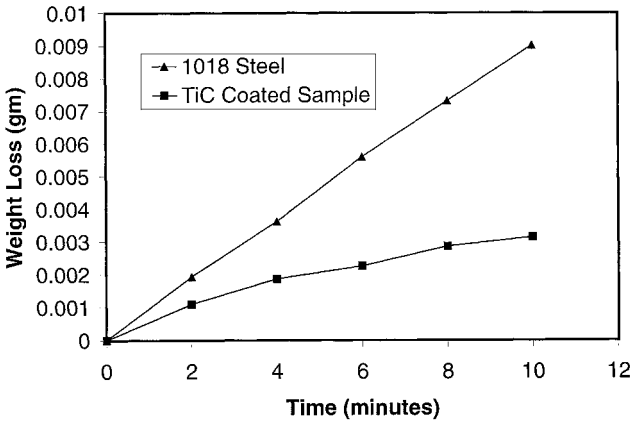

Fig. 9 Variation in cumulative weight loss as a function of time during dry sliding test

nature of the coating, as discussed earlier. There is no indication of brittle failure or loose debris formation of the TiC ceramic phase. The wear phenomenon in such multiphase composite materials is fairly complex, depending on several factors such as volume fraction, distribution, and morphology of the carbide particles (Ref 25). Under ideal conditions, monolithic ceramics such as TiC are supposed to fail in a brittle manner under wear conditions (Ref 26). However, the presence of softer phases such as ferrite and austenite (as observed in x-ray diffraction spectrum in Fig. 7) between hard ceramic particles alters the wear nature of monolithic TiC. It has been mentioned earlier that Fe acts as an excellent binder for Ti-base refractory ceramics (Ref 17, 20). This prevents debonding at the TiC particle/Fe matrix interface. Also, as mentioned earlier, several of the TiC islands in Fe matrix are formed in an in situ manner during the coating process, providing a coherent interface between these islands and the matrix (Fig. 4a and 5). Under such wear conditions, Fe-base matrix phases deform plastically to accommodate the high stresses experienced by TiC particles. This prevents brittle fracture and fragmentation of TiC ceramic particles. Hence, chipping off is prevented, and no loose debris is observed in Fig. 10. A composite film containing hard TiC particles and soft Fe phases covers the entire substrate, which assists in reducing the wear rate. The x-ray diffraction spectrum of a worn surface is shown in Fig. 7. Within the limits of resolution of the x-ray diffractometer, the spectrum does not indicate evolution of any new phases during the wear process. Such new phases, if formed, could influence the wear behavior of the coatings.

Coefficient of Friction Measurement. In the present work, the coefficient of friction is calculated by measuring the changes in voltage and current in the electrical circuit of the motor driving the block-on-ring tribometer during loading (Ref 27). Based on the principle of energy conservation, the frictional energy (W_f) equals the change in the electrical work during loading, as given by Eq 1.

$$W_f = \text{voltage } (\Delta V) \times \text{current } (\Delta I) \quad \text{(Eq 1)}$$

From friction theory, it is known that:

$$W_f = \Delta N v \quad \text{(Eq 2)}$$

where N is normal load, v is the linear speed of the disk, and μ is the coefficient of friction. By equating above the two equations, the coefficient of friction is computed. The measurement of coefficient of friction provides direct information about the work done to deform (elastically and/or plastically) the surface material. However, it is not necessarily a direct indication of material loss or separation as loose debris from the surface. Also, high friction does not necessarily imply high wear rate (Ref 28).

The computed coefficient of friction for TiC coating has been plotted for the entire test time of 10 min (Fig. 11). Coefficient of friction values are constant and do not fluctuate significantly. The best fit line shows the coefficient of friction to be 0.58. Such behavior of the composite coating could be explained by a model that illustrates frictional behavior of multiphase and /or composite materials (Ref 25).

This model predicts that friction of a composite/multiphase material is influenced by the relative amounts and friction coefficients of the constituent phase. Also, friction is affected by the wear resistance of an individual constituent. In most wear situations, the more wear resistant phases carry a disproportionately larger part of the load and hence have a larger influence on the friction of the composite. Hence, the friction coefficient of the composite generally does not follow a linear rule of mixture but is dominated by the friction coefficient of the most wear-resistant constituent. It is well understood that a refractory ceramic like TiC has high wear resistance as compared to that of plain carbon steel. Hence, according to the model discussed above, TiC particles in the coating tend to carry a larger load than Fe and contribute largely toward the coefficient of friction of the composite coating. It has been proposed earlier that TiC coatings have a low coefficient of friction and are ideal candidates as solid lubricants for high vacuum applications (Ref 2). Because TiC has a high wear resistance and low coefficient of friction, it dominates the friction of the composite. Such a hypothesis is supported by Fig. 10, which shows a composite film of TiC and Fe on the worn surface. Formation of such a film leads to an earlier stabilization of coefficient of friction, which is evident from Fig. 11.

4. Conclusions

- An ultrahard TiC coating has been successfully deposited over AISI 1018 steel using a high energy density process such as PES. The coating is adherent, crack free, and defect free. However, coating thickness is not uniform, which is a characteristic feature of PES process.
- The coating is composite in nature with TiC being the most stable phase in a Fe-rich matrix. Islands of TiC of various sizes and shapes are present in the coating. Such coating morphology is due to the highly active and complex Fe-Ti-C material system.
- A coating with high hardness value is obtained.
- Wear resistance of the coated surface has increased significantly. The wear behavior of the TiC coated surface is explained by formation of a composite film, which accommodates stresses by plastic deformation of softer phases.
- A coefficient of friction has been computed and explained on a model based on the composite/multiphase material.

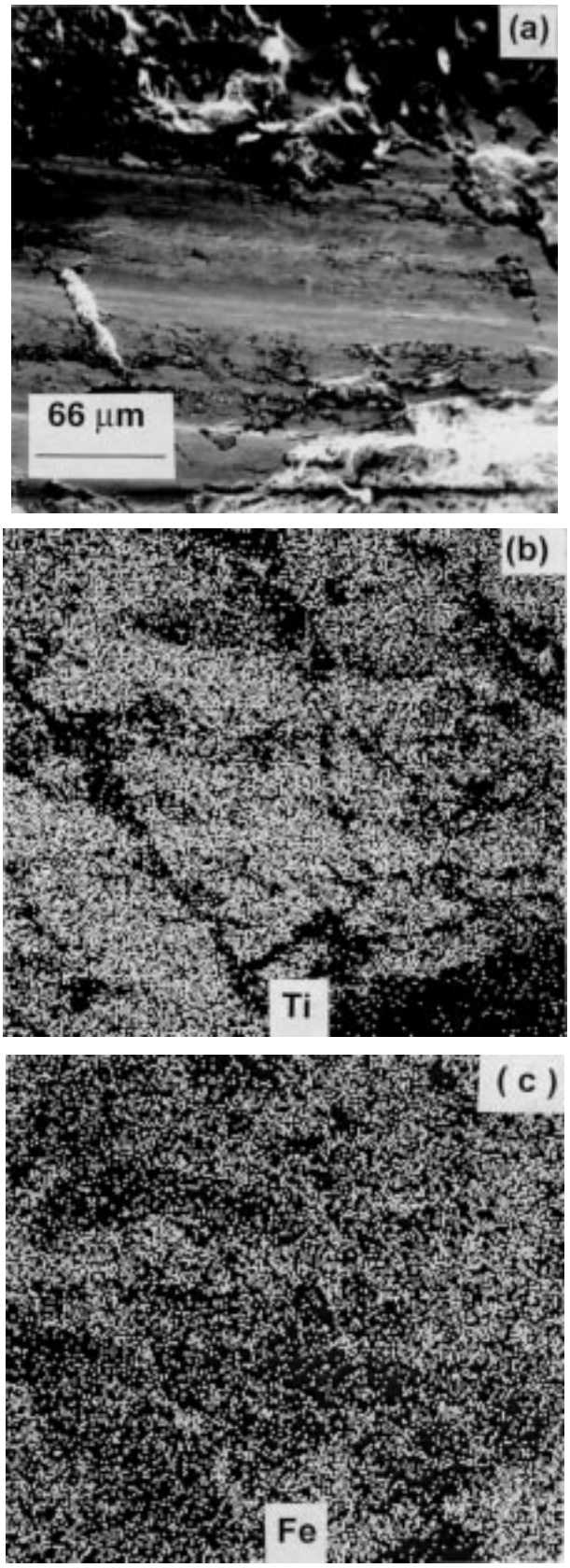

Fig. 10 (a) SEM micrograph of the worn surface of TiC coated steel coupon and corresponding x-ray elemental map for (b) Ti and (c) Fe

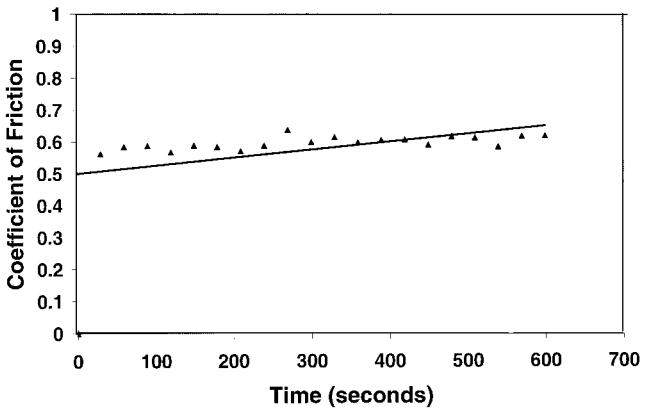

Fig. 11 Variation in coefficient of friction with time during dry sliding test

Acknowledgments

The authors thank Dr. T.S. Sudarshan at Materials Modifications Inc. (MMI), Fairfax for supplying the coated samples and Mr. R. Raman and Mr. S. Krupashankar, also at MMI, who extended support in depositing the coating by PES technique. The authors acknowledge financial support from the U.S. Air Force (contract No. F 40600-96-C-0004) for this work.

References

1. T.Y. Kosolapova, *Carbides: Properties, Production and Applications,* Plenum Press, New York, 1971, p 97-122
2. K. Upadhya, Properties and Performance of Plasma-Assisted Physically Vapor Deposited TiC Coatings, *Mater. Sci. Eng. A,* Vol 140, 1991, p 549-553
3. S. Kinkel, G.N. Angelopoulos, and W. Dahl, Formation of TiC Coatings on Steel by a Fluidized Bed Chemical Vapor Deposition Process, *Surf. Coat. Technol.,* Vol 64, 1994, p 119-125
4. M.L.F. Parames and O. Conde, Structure and Morphology of Laser Assisted Chemical Vapor Deposited TiC Coatings, *J. Phys. (France) IV,* Vol 3, 1993, p 217-224
5. R.N. Johnson, Principles and Applications of Electro-Spark Deposition, *Surface Modification Technologies,* T.S. Sudarshan and D.G. Bhat, Ed., The Metallurgical Society, 1988, p 189-213
6. R.N. Johnson, Electro-Spark Deposited Coatings for High Temperature Wear and Corrosion Applications, *Elevated Temperature Science and Technology I,* N.B. Dahotre, J.M. Hampkian, and J.J. Stiglich, Ed., The Minerals, Metal and Materials Society, 1995, p 265-277
7. E.A. Brown, G.L. Sheldon, and A.E. Bayoumi, A Parametric Study of Improving Tool Life by Electrospark Deposition, *Wear,* Vol 138, 1990, p 137-151
8. G.V. Samsonov, A.D. Verkhoturov, V.S. Sychev, and A.I. Bezykornov, Investigation of Some of the Laws Governing the Formation of a Hardened Layer during the Process of Electric-Spark Alloying, *Fiziko-Khimicheskaya Mekhanika Materialov,* Vol 7 (No. 5), 1971, p 3-6
9. K. Natesan and R.N. Johnson, Corrosion Resistance of Chromium Carbide Coatings in Oxygen-Sulfur Environment, *Surf. Coating Technol.,* Vol 33, 1987, p 3411-3451
10. R.N. Johnson, Coatings for Fast Breeder Reactor Components, *Thin Solid Films,* Vol 118, 1984, p 31-47
11. S. Raghunathan, J.J. Stiglich, and T.S. Sudarshan, Characterization of Ir/Re Duplex Coatings on Ta/10W Deposited by Pulsed Electrode Surfacing (PES), *Elevated Temperature Science and Technology I,* N.B. Dahotre, J.M. Hampkian, and J.J.

Stiglich, Ed., The Minerals, Metals and Materials Society, 1995, p 303-312

12. N.B. Dahotre, M.H. McCay, and T.D. McCay, Diamond Materials for Electromagnetic Railguns, *Mater. Manuf. Process.*, Vol 9 (No. 1), 1994, p 1-36
13. N. Frage, L. Levin, E. Manor, R. Shneck, and J. Zabicky, Iron-Titanium-Carbon System. I. Equilibrium Between Titanium Carbide (TiC_x) of Various Stoichiometries and Iron-Carbon Alloys, *Scr. Mater.*, Vol 35 (No. 7), 1996, p 791-797
14. C. Raghunath, M.S. Bhat, and P.K. Rohatgi, In Situ Technique for Synthesizing Fe-TiC Composites, *Scr. Metall.*, Vol 32 (No. 4), 1995, p 577-582
15. S. Jonsson, Assessment of the Fe-Ti-C System, Calculation of the Fe-Ti-N System and Prediction of the Solubility Limit of Ti (C,N) in Liquid Fe, *Metall. Mater. Trans. B*, Vol 29, 1998, p 371-384
16. N. Frage, L. Levin, E. Manor, R. Shneck, and J. Zabicky, Iron-Titanium-Carbon System. II. Microstructure of Titanium Carbide (TiC_x) of Various Stoichiometries Infiltrated with Iron-Carbon Alloy, *Scr. Mater.*, Vol 35 (No. 7), 1996, p 799-803
17. A. Agarwal and N.B. Dahotre, Pulse Electrode Deposition of Superhard Boride Coating on Ferrous Alloy, *Surf. Coat. Technol.*, Vol 106 (2/3), 1998, p 242-250
18. *Alloy Phase Diagrams*, Vol 3, *ASM Handbook*, ASM International, 1992
19. G.V. Samsonov and I.M. Vinitskii, *Handbook of Refractory Compounds*, IFI Plenum Data Company, New York, 1980, p 138-140
20. A.A. Ogwu and T. J. Davies, Electronic Structure Basis for Selection of Metal Binders for Hardmetal Systems, *Mater. Sci. Technol.*, Vol 9, 1993, p 231-217
21. G.S. Upadhyaya, Wetting of Ceramic by Metal Melts: An Electronic Approach, *Sintered Metal-Ceramic Composites*, G.S. Upadhyaya, Ed., Elsevier Science Publishers, Amsterdam, 1984, p 41-50
22. S. Economou, M. De Bonte, J.P. Celis, J.R. Ruos, R.W. Smith, E. Lugscheider, and A. Valencic, Tribological Behavior of TiC/TaC-Reinforced Cermet Plasma Sprayed Coatings Tested Against Sapphire, *Wear*, Vol 185, 1995, p 93-110
23. L. Ramquist, *Int. J. Powder Metall.*, Vol 4, 1965, p 1-4
24. P.H. Booker, Ph.D. thesis, Oregon Graduate Center, 1979
25. N. Axen, I.M. Hutchings, and S. Jacobson, A Model for the Friction of Multiphase Materials in Abrasion, *Tribol. Int.*, Vol 29 (No. 6), 1996, p 467-475
26. W.A. Glaeser, Friction and Wear of Ceramics, *Friction, Lubrication, and Wear Technology*, Vol 18, *ASM Handbook*, ASM International, 1992
27. P.K. Rohatgi, N.B. Dahotre, Y. Liu, M. Yin, and T.L. Barr, Tribological Behavior of Al Alloy-Graphite and Al Alloy-Microcrystalline Carbon Particle Composites, *Proc. International Symposium on Advances in Cast Reinforced Metal Composites*, S.G. Fishman and A.K. Dhingra, Ed., ASM International, 1988, p 367-373
28. J. Halling, Tribology, *Surface Treatment for Protection: Spring Review Course*, The Institution of Metallurgists, Great Britain, Series 3 (No. 10), 1978, p 118-129